Time-resolved backside optical probing of picosecond-laser-pulse-produced plasma in solid materials

Brian-Tinh V. Vu
Department of Applied Science, University of California at Davis, Livermore, California 94550
and Lawrence Livermore National Laboratory, Livermore, California 94550

Otto L. Landen and Abraham Szoke
Lawrence Livermore National Laboratory, Livermore, California 94550
(Received 9 November 1992)

We report on pump-probe measurements of reflectivity and transmissivity of a plasma produced in transparent solid materials. The plasma is created by irradiating uncoated transparent planar glass targets with 1.0-ps FWHM laser pulses at a peak intensity of 2.0×10^{13} W/cm^2. Time-resolved measurements using a probe light pulse incident from the backside are presented, revealing two competing mechanisms: one is highly absorptive due to a bulk underdense plasma formed behind the target surface, and the other is highly reflective due to an overdense plasma layer at the surface. A simple self-consistent and analytical model, similar to the avalanche model, is proposed, leading to both time-dependent and time-integrated solutions to the evolution of plasma density profiles and characteristics of high-intensity-laser-pulse propagation and absorption in the transparent material. Calculations of the probe light interacting with this plasma show that excellent agreement with experimental measurements can only be obtained by including a contribution from the bulk plasma formed behind the surface. Experimental measurements with Au-coated targets are also shown to illustrate elimination of the bulk plasma.

PACS number(s): 52.50.Jm, 52.70.Kz, 52.40.Db, 52.65.+z

I. INTRODUCTION

Recent studies of plasmas produced by ultrashort laser pulses have stimulated great interest in both unexplored physics of high-density and -temperature plasmas and its potential applications in the development of x-ray lasers or x-ray sources of high brightness [1–4]. The plasma produced by irradiation of a transparent solid target with an intense ps laser pulse, in several important physical aspects, is different from plasmas that are created by laser pulses of ns duration or longer. For example, transparent targets eliminate the effect of a laser prepulse that otherwise may be sufficient to preionize and ablate the target surface prior to the arrival of the main pulse [5]. Also, since absorption and electron heating take place within the short duration of the pulse, there is very little or greatly reduced effect due to hydrodynamic expansion into surrounding vacuum during the heating pulse [6–9], thus allowing us to interrogate or probe the plasma before its expansion. The scale length of such plasma at the front target surface is of the order of the optical skin depth ($c_s\tau_p\sim100$ Å), much smaller than the laser wavelength (~5800 Å). Hence, this lessens the complications due to nonlinear processes such as stimulated Brillouin and Raman scatterings, or profile steepening in the laser-plasma interaction that are all associated with long-scale-length plasmas [10]. Moreover, the backside probing in our pump-probe scheme with transparent targets advantageously avoids these complications altogether. The reason is that the plasma, as seen from the backside, is enveloped by a well-defined solid surrounding it and experiences essentially no hydrodynamic expansion. The plasma is then allowed to interact with the probe light, whose intensity is kept below the thresholds for growth rates of nonlinear processes [10]. Another advantage of backside probing is that, unlike frontside probing, where the probe light is reflected off the overdense plasma layer at the surface and does not sense the ionized region behind it, backside probing can provide answers as to how the laser energy is coupled and transported into the bulk transparent region. These questions are important in most laser fusion experiments, where laser-plasma coupling and transport mechanisms critically determine both the plasma conditions and the efficiency of target implosion [11,12].

In this paper, we discuss a pump-probe experiment in an attempt to characterize the mechanisms accounting for plasma formation as a result of irradiation of a transparent target surface with a high-intensity (pump) pulse. Time-resolved measurements of reflectivity and transmissivity in backside probing of this plasma are presented together with a discussion of a simple self-consistent model. The model provides both time-dependent and time-integrated analytical solutions to the evolution of the plasma density and laser-pulse profile inside the transparent solid. Characteristics of high-intensity laser-pulse propagation and absorption are discussed in detail. Simulation results of the probe light interacting with the plasma imbedded in the solid show excellent agreement with experimental data when absorption by the bulk underdense plasma is taken into account to offset the high reflectivity of the surface overdense plasma. Also, measurements with Au-coated targets are presented, demonstrating the disappearance of the bulk plasma.

II. EXPERIMENTAL DETAILS AND SETUP

The laser system consists of a dye oscillator synchronously pumped by a frequency-doubled cw mode-locked Nd:YAG oscillator operating at a rate of 125 MHz [13]. Dye pulses of about 2-nJ energy from the oscillator are then amplified by a sequence of three high-gain dye cells pumped at 10 Hz by a frequency-doubled Q-switched Nd:YAG laser. The fluence of prepulse accompanying the main pulse are kept below 0.1 J/cm^2 to prevent formation of a long-scale-length and low-density plasma before arrival of the main pulse. The mode-locked dye oscillator normally produces a post pulse which accounts for 10% of the total energy. It has been effectively suppressed by a factor of ≈ 30 by a gain-quenching scheme implemented at the first dye amplifier cell [14]. The energy per pulse is ~ 1.5 mJ and the wavelength is 580 nm. Figure 1 shows a measured autocorrelation trace normalized to peak intensity. It is best fit to a normalized second-order autocorrelation, assuming a sech^2 temporal shape with a full width at half maximum (FWHM) of 1.0 ps.

The experimental setup, as shown in Fig. 2, is housed inside a vacuum chamber with pressure maintained at $\approx 10^{-5}$ torr. The laser pulse is divided, by a 1% beam splitter, into a stronger pump pulse and a weaker probe pulse. The target is a commercially made glass slide, consisting of 72.6% SiO_2 and 27.4% impurities [15]. The mass density is $\rho = 2.2$ g/cm^3 and linear refractive index is $n_g = 1.52$. The focusing spherical lenses are 25- and 7.5-cm focal length for the pump and the probe beam, respectively. The probe is tightly focused to a spot of 25-μm diam and centered on the larger focused pump spot of 75-μm diam. Polarization of the probe is s-polarized, orthogonal to that of the pump, so that stray diffuse light from the pump may be rejected using polarizers before detection. The pump beam is normal to the target with a peak spatially averaged intensity kept at 2.0×10^{13} W/cm^2. The incidence angle of the probe is 30° to the normal at the rear surface, corresponding to an internal angle of 19° at the front surface. This angle fixes the length of the interaction region at ≈ 100 μm, much smaller than the Rayleigh ranges of the pump (7 mm) and probe (0.8 mm) beams. The probe intensity is kept at the level of $\approx 2.0 \times 10^{10}$ W/cm^2, sufficiently low to be nonintrusive but still sufficiently high to discriminate the probe pulse specular reflection from the diffusely scattered light of the intense pump pulse. Timing of the probe relative to the pump is varied by a computer-driven delay line with 1-μm accuracy in increments equivalent to 24.5 fs between laser shots. Velocity nonlinearity and other inaccuracies in the translation stage are all negligible compared to the spatial extent of the laser pulse (≈ 300 μm). A mechanical raster system translates the target between laser pulses so that each laser pulse arrives at a fresh part of the target. Spatial walkoff between the pump and probe beams at the target surface is kept below an acceptable 20 μm throughout a temporal scan as follows: The unamplified transmitted probe beam is viewed through a damage crater formed previously by the pump beam as the target is rastered. The horizontal and vertical tilt of the target are adjusted until the probe beam tracks the crater throughout a 5×5cm^2 raster. The walkoff, translation-stage wobble, and timing errors (< 100 fs) due to target-thickness variations are all negligible, thus ensuring the same conditions of plasma formation and probing on each laser short. p-i-n diodes are used to simultaneously monitor incident, specular reflection and transmission signals of the probe. These signals are preamplified and sent to gated boxcar integrators interfaced with a computer for storage and further data reduction.

Rough absolute timing to within 20 ps between the probe and the pump pulses is obtained with a fast photodiode. To determine the zero timing between the two initially counterpropagating pulses with better accuracy, we have performed induced phase modulation measurements

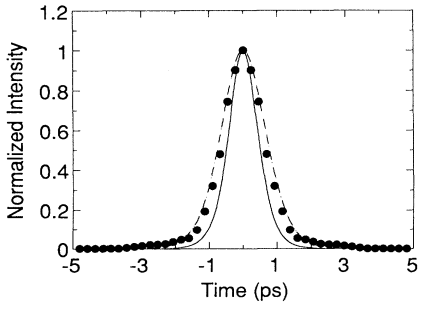

FIG. 1. Measured autocorrelation trace of the laser-pulse intensity (closed circles) normalized to peak intensity. A laser pulse with a 1.0-ps FWHM and sech^2 shape (solid curve) is assumed and yields the best-fit autocorrelation (dashed curve), in least-square sense, to the measured trace.

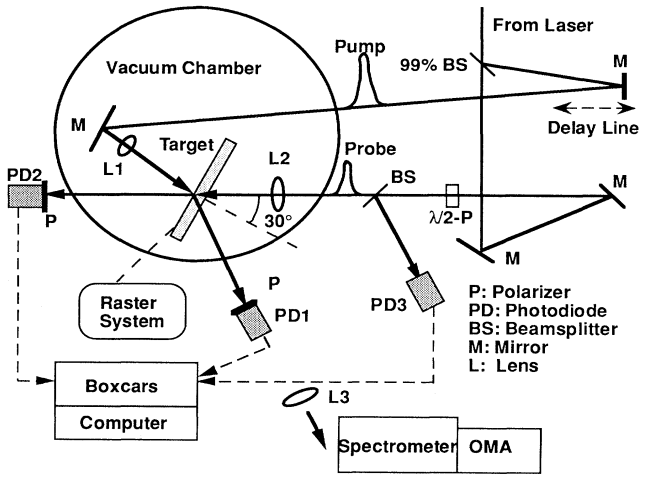

FIG. 2. Details of the pump-probe experiments. Backside probing of the plasma in a transparent target is studied by time-resolved measurements of reflectivity and transmissivity that are simultaneously monitored by p-i-n diodes. Spectral changes in the reflected probe light are resolved by a spectrometer and an optical multichannel analyzer to infer absolute zero time of the two pulses.

[16]. In these spectral measurements, the pump intensity is reduced to $\approx 1\times 10^{12}$ W/cm^2, below the plasma formation threshold, but still sufficiently strong to induce a modulation in the refractive index of the glass medium, which is given by $n_g(t)=n_{0g}+n_{2g}I(t)$, where n_{0g} and n_{2g} are the linear and nonlinear refractive indices, respectively, and $I(t)$ is the instantaneous intensity of the pump pulse. The spectral shifts of the reflected probe light are then resolved by a spectrometer interfaced with an optical multichannel analyzer. The shifts for the return journey of the reflected probe light are seen to be proportional to the time derivative of the pump intensity. At early delay time, or during the rising edge of the pump pulse, the probe suffers a red shift. At late delay time, or during the falling edge, the probe experiences a blue shift. When the two pulses are perfectly overlapped in time at the surface, defined as the absolute-zero delay time, there is no spectral shift observed in the probe light. The above is generally true for the probe pulse copropagating with the pump pulse [17]. However, during its arrival to the front surface, the counterpropagating probe experiences an additional shift that is proportional to the accumulation of phase change as it traverses the pump-pulse profile. Analysis of the spectral measurements shows that by correcting the frequency shifts in the probe on its copropagating (return) journey for shifts accumulated during its counterpropagating (arrival) journey, we can determine the location of the absolute-zero timing to within 0.2 ps [18].

III. EXPERIMENTAL RESULTS AND DISCUSSION

Figure 3 shows simultaneous scans of reflectivity and transmissivity as functions of relative delay time for uncoated targets. Each experimental data point is a single shot measurement. The data have been first divided by the incident energy (3% rms fluctuation). From the reflection data we then subtracted an average 0.15% of the incident probe light for diffuse pump light scattered into the reflection diode ($PD1$), and 4.0% for the probe light reflected from the undisturbed backside surface. The data was then normalized to an absolute value of 3.7% reflectivity for the cold target. Similarly, subtracting an average 14.0% for diffuse pump light scattered into the transmission diode ($PD2$), transmission data was normalized to a value of 92.3% transmissivity for the cold target. Absolute-zero-time-delay position is determined from the induced-phase-modulation experiments with the same experimental conditions except that the pump intensity level is attenuated below the plasma formation threshold. Note that zero timing is when the peaks of two pulses overlap at the front surface.

In both data scans, the plateaus during early or large negative delay time correspond to values for the undisturbed target where the probe arrives prior to the pump. Following the plateaus, both curves exhibit a transient fall time of about 2 ps. The decrease in reflection data occurs about 0.5 ps before the decrease in transmission. At late delay time, both reflection and transmission of the probe again show constant levels. The remaining small fluctuations in the data points are attributed to fluctuations in the pump stray light which does not track the pump energy and to background electronic noise in the boxcar integrators. At much later delay, many s after plasma formation when the plasma has completely recombined leaving the surface annealed, the reflectivity and transmissivity are found to be similar to that of the undisturbed target, albeit with some small decrease ($\approx -0.9\%$ in reflection and $\approx -7.0\%$ in transmission) due to asperity of the annealed surface.

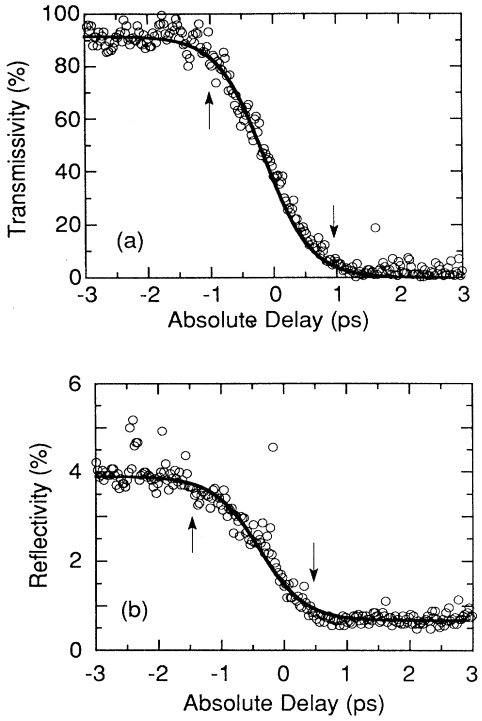

FIG. 3. Simultaneous scans of (a) transmission and (b) reflection taken with uncoated targets (open circles). Solid curves are from the model discussed in text. Absolute-zero time is determined from induced phase modulation measurements, as discussed in text. Arrows mark the beginnings and endings of the transients corresponding to points of 10% difference from the plateau levels.

The temporal behavior observed in the probe reflection and transmission can be qualitatively understood by considering the sequence of events as the pump pulse arrives at the target surface: At early time or during the leading edge of the pump pulse, where the intensity at the surface is low, nearly 96% of the light is transmitted through the front surface. As the transmitted pump light propagates into the bulk region, it is absorbed and ionizes the transparent material, resulting in a bulk underdense plasma behind the surface. Since the density of the undercritical plasma ($<N_{cr}=3.3\times 10^{21}$ cm^{-3}) is much below solid density ($N_a=6.6\times 10^{22}$ cm^{-3}), ionization of neutral atoms is the main contribution to the formation of the plasma [19,20]. The velocity of the ionization front should be $\approx cn_0/n_g^2$, where c is the speed of light, and the refractive index in the region swept through by the ion-

ization front is $n_0 \approx (n_g^2 - N_e/N_{cr})^{1/2} \approx n_g$. ($N_e$ is the number density of electrons.) The spatial steepness of the leading edge of the ionization front depends on the rise time of the laser profile at the intensity level which produces such an electron density. At some time t_{cr}, there is a critical-density plasma layer formed at the surface. As this plasma layer becomes thick enough (≈ 0.1 μm), it completely stops further pump-pulse transmission. As a result, the remaining pump light is kept from further interacting with the bulk region behind the surface plasma layer, and instead deposits its energy at the surface plasma layer, quickly producing a thin region of highly reflecting, solid-density plasma [21]. The transmitted portion of the pump pulse continues deeper into the target, ionizing until it exits at the rear surface. Thus, at late time there are two competing mechanisms for the backside probe pulse: One is highly reflective due to the formation of a steep overdense layer at the surface, the other is strongly absorptive due to a bulk underdense plasma produced behind the surface.

In view of this picture, we explain the temporal behavior of the probe data as follows. At early delay, prior to the critical time t_{cr}, there is a small underdense plasma which causes little absorption in the transmitted probe during its incoming journey to the front surface. The probe light reflected from the surface, however, will copropagate with the ionization front and hence suffer additional absorption over a maximum interaction length of 100 μm on its return journey. This accounts for the earlier decrease in the reflected light. Thus the time at which the reflection transient begins should determine, after convolution with the probe-pulse profile, the time at which a plasma of an appreciable density is formed by the leading edge of the ionization front. As will be seen later, this density of about 10^{18} cm^{-3} reduces probe reflection by 10% from the value of the cold target. At the critical time t_{cr}, the probe transmission is completely turned off by formation of a critical-density plasma and subsequently a surface overdense layer. By contrast, the probe reflection may be enhanced by the surface plasma layer, only to be heavily absorbed again by the bulk plasma on its return journey. At the start of the reflection transient, it is the trailing edge of the probe pulse that is absorbed appreciably. The end of the transmission transient occurs when the leading edge of the probe pulse sees the surface critical plasma. Therefore, the time lag of ≈ 2.5 ps between the beginning of reflection transient and the end of the transmission transient is the estimate of the time lapse, convolved by the probe pulse length, between the formation at the surface of an appreciable density plasma and critical plasma, and this time lapse, as will be shown later, is about 0.14 ps. Since the time scales for cooling and hence recombination in the underdense plasma by electron-atom and electron-ion collisions are > 100 ps [19,20,22], these processes can be neglected on the few-ps time scale of Fig. 3. Also, measurements with Au-coated targets described below (Fig. 4) confirm that surface plasma reflectivity remains approximately unchanged over the time scale of few ps. For these reasons, the final reflection and transmission levels of the probe light should also remain approximately constant, as is observed.

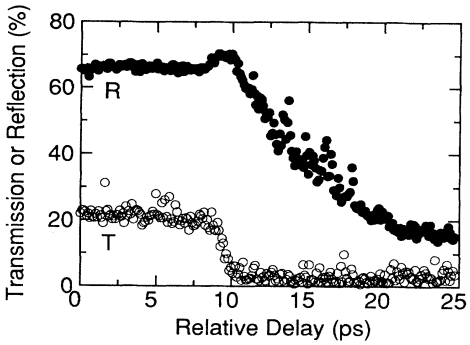

FIG. 4. Simultaneous scans of reflectivity (closed circles) and transmissivity (open circles) for Au-coated targets. Unlike uncoated targets, reflection enhancement is seen as an indication of elimination of absorption by an underdense plasma.

Specifically, to isolate the effects of such a highly reflecting surface overdense plasma, we have performed the same experiments with the glass targets overcoated with an absorptive gold film of 300-Å thickness at the front surface. The target was also antireflection coated on its rear surface to enhance the contrast in the reflection data between early and late time delay. The use of the Au coating is to promote larger absorption of the intense pump pulse at the surface, leading to an earlier formation of a surface overdense plasma, hence preventing formation of the bulk underdense plasma behind the coating. An estimate of the critical intensity level at which the Au region reaches critical density gives a value of $\approx 4 \times 10^{11}$ W/cm^2. As will be seen later, the bulk plasma produced in the glass by the transmitted pump pulse at this intensity level is of negligible density. The absorption of the cold Au layer is $\approx 12\%$, inferred from values of 64% reflectivity and 24% transmissivity that are measured by the probe. The data, as displayed in Fig. 4, taken in the same manner described above were normalized to reflectivity and transmissivity of the cold target. The data shows a transmission transient time of 2.0 ps, about the same as that of uncoated targets. At the same time delay, however, there is a reflection enhancement of nearly 10% of about 2.0-ps duration. Following the reflection enhancement is a long reflection decrease with $1/e$ decay time of about 8.0 ps. This behavior proves that with Au-coated targets we have succeeded in isolating the highly reflective surface overdense plasma layer from large absorption by a bulk underdense plasma. Further detailed discussion of measurements and calculations for Au-coated targets, taking into account the effects of thermal heat wave propagation [8,20] to explain the slow decay in reflectivity, will be given in a future publication.

IV. THEORETICAL MODEL AND CALCULATIONS

In order to model self-consistently the time evolution of the bulk underdense plasma in space as described

above, we propose the following equations (in cgs units):

$$\frac{1}{v_g}\frac{\partial I(x,t)}{\partial t}+\frac{\partial I(x,t)}{\partial x}=-N_a\sigma_\nu(x,t)I(x,t)$$
$$\equiv -bN_e(x,t)I(x,t)\ , \tag{1}$$

$$(E_i+\tfrac{3}{2}kT_e)\frac{\partial N_e}{\partial t}+\tfrac{3}{2}kN_e\frac{\partial T_e}{\partial t}=N_a\sigma_\nu(x,t)I(x,t)$$
$$+[-D\nabla^2(N_e\tfrac{3}{2}kT_e)$$
$$-\tfrac{3}{2}kN_e(T_e-T_a)\nu_{ea}]\ . \tag{2}$$

Equation (1) is the transport equation for a wave packet of laser photons traveling in a transparent medium with a group velocity $v_g\approx c/n_g$ and an absorption coefficient κ equal to the product $N_a\sigma_\nu$. N_a is number density of neutral atoms. σ_ν is the cross section for free-free absorption of a photon during an electron-atom collision and is linearly proportional to electron density [19], $\sigma_\nu=bN_e/N_a$, where b is defined as the cross section at solid density. Equation (1) describes characteristics of laser-pulse propagation and absorption in the transparent medium: as it propagates it is absorbed and attenuated, imparting energy to heating of the free electrons. Consequently, deformation of the pulse profile occurs. Early during the leading edge of the pulse when the electron density is still low, the effect on the profile is small. At later time, the increasing-density plasma has a greater effect on the profile. More details on the characteristics of the laser-pulse propagation are given in the Appendix.

Similar to the initiation of breakdown in solid materials by an avalanche process [23–26], creation of electron density begins with a small number N_{e0} of free electrons that are generated by multiphoton processes or by readily ionized impurity atoms. When these initial electrons gain sufficient kinetic energy $3kT_e/2$ from the laser field, they collide with nearby atoms to produce a cascade of secondary electrons. Equation (2), similar to that of the Harrach model [27], describes the evolution of electron plasma with E_i as ionization energy except for an additional term due to spatial diffusion of electrons out of the interaction region. On the few-ps time scale, energy losses due to ambipolar diffusion ($\approx$100 ps for a diffusion scale of 1000 Å), lateral electron thermal conduction or free streaming diffusion ($\approx$100 ps) [19], and the radiative cooling time ($\approx$100 ns) [22] can be all safely ignored. The second term in the bracket for energy exchange in direct electron-atom collisions can also be neglected by virtue of the long characteristic time ($\approx$1 ns) for appreciable energy transfer in electron-atom collisions.

According to Harrach's model, the plasma formation and heating process reveal two distinct stages [27,28]. The first stage is the heating of initially free electrons to some high characteristic temperature, followed by a stage of ionization growth in which collisions between hot electrons and atoms prevent further temperature change. The model gives an estimate of $\approx$10 fs for the characteristic heating time and the characteristic temperature of $\approx$1.0 eV at 10^{13} W/cm^2 intensity. For our experimental conditions we therefore neglect the term in $\partial T_e/\partial t$, and assume a maximum final temperature of 1.0 eV that is given by the Saha equation for $E_i=9$ eV, $N_e\le N_{\rm cr}$ and $N_{\rm cr}=N_a/20$. Another way to justify omission of this term is by examining Eq. (2) without terms in the bracket. The electron density grows exponentially with a growth rate proportional to the intensity, whereas temperature only increases as some power of intensity, and this power dependence is less than one, since ionization competes with the heating process. A physical implication of this approximation is analogous to that given by Newstein [28]: Under the influence of the laser field, at some characteristic time the free electrons gain as much energy from the field as they lose to many cold electrons that are bound to the nearby atoms. Thus there is a steady state in which further heating is balanced by the rate of energy lost to ionizing neutral atoms. As a result, energy absorbed during the subsequently arriving pump pulse does not give rise to any further significant temperature increase, but instead goes toward the predominant ionization of atoms. For these reasons we can also then neglect the temperature dependence of the electron-atom collision cross section.

Equation (2) preserves the exponential nature of the avalanche model, where the ionization rate coefficient is linearly proportional to the laser intensity and electron density is a steeply rising function of intensity. Therefore, the critical threshold $I_{\rm cr}=I(0,t_{\rm cr})$ and critical time $t_{\rm cr}$ are weakly dependent or essentially independent of the initial condition $N_{e0}(x)$. Hence, early during the leading edge of the laser pulse, details of any ionization process other than collisional ionization, such as multiphoton, photoionization of impurities, or F-center formation, are unimportant and just serve to produce a number of "priming" electrons $N_{e0}(x)$, initiating the subsequent cascade processes in the interaction region [23,25,26].

Interestingly, Eq. (2) with the terms discussed above neglected together with Eq. (1) are analogous to those of Frantz and Nodvik [29] for laser amplification, except we describe here propagation of high-intensity laser pulse in an absorptive medium, with an absorption that depends exponentially on the laser intensity. Solving the two equations by the method of characteristics with an input laser pulse $I_0(t)=I(0,t)$ at the surface and an initial electron density $N_{e0}(x)=N_e(x,-\infty)$, time-dependent solutions to the electron-density evolution and laser pulse propagation are, with $I_0(t\ge t_{\rm cr})$, set to 0 to simulate formation of the surface critical plasma, given by

$$I(x,t)=\frac{I_0\left[t-\dfrac{x}{v_g}\right]}{1+\exp\left[a\displaystyle\int_{-\infty}^{t-x/v_g}I_0(t')dt'\right]\left[\exp\left[b\displaystyle\int_0^x N_{e0}(x')dx'\right]-1\right]}\ , \tag{1'}$$

$$N_e(x,t)=\frac{N_{e0}(x)}{1+\exp\left[-b\int_0^x N_{e0}(x')dx'\right]\left[\exp\left[-a\int_{-\infty}^{t-x/v_g} I_0(t')dt'\right]-1\right]}, \quad (2')$$

where the proportionality constant $a=b/(E_i+\frac{3}{2}kT_e)$.

The time evolution, from -3.0 to $+3.0$ ps, of electron density normalized to the critical density is shown in Fig. 5. The pump pulse (not shown in the figure) is incident onto the target surface ($x=0$) from the left. Note that zero time refers to the time when the peak of the pulse arrives at the surface. Parameters used for the calculation are the following: peak intensity $I_{\text{peak}}=2.0\times10^{13}$ W/cm^2 with a sech^2 profile and FWHM$=1.2$ ps; $T_e=1.0$ eV; $b=1.2\times10^{-17}$ cm^2. Ionization energy is taken as the energy gap ($=9$ eV) between the valence and conduction bands of the insulator material. We take $N_{e0}=10^8$ cm^{-3}, a typical value often used in previous works on laser-induced damage [26,30]. This number corresponds to $\approx$ ten initial electrons in the interaction volume of $\approx10^{-7}$ cm^{-3}.

The critical plasma layer formed at the surface takes place during the leading edge of the pulse, at $t_{\text{cr}}=-0.46$ ps and $I_{\text{cr}}=1.3\times10^{13}$ W/cm^2. The calculation shows the time lapse for the density growth at the surface from a density of 10^{18} cm^{-3} to N_{cr} is $\Delta t=0.14$ ps. Prior to the critical time t_{cr}, the plasma-buildup rate is given by Eq. (2), $N_e'/N_e=aI(x,t)$, an increasing function of time up to a maximum at t_{cr} which sets an upper limit for the peak intensity of the transmitted pump pulse. At time $t>t_{\text{cr}}$ an underdense plasma plateau of $\approx10^{19}$ cm^{-3} begins to develop inside the bulk region as the transmitted pump continues to the rear surface ($x=1000$ μm). The average plateau density is about 330 times below the critical density and about 6000 times less than the solid density.

Comparisons of ionization rates with previous measurements obtained from the laser-induced damage studies on NaCl crystals by laser pulses of 20 ps and longer duration are plotted in Fig. 6 against the critical or threshold electric field [23,24]. The experimental data (open circles) together with the semiempirical calculations (dashed curve) are taken from Bloembergen [24]. The curve was derived with an assumption that the free-electron mobility is independent of the electric field, and it shows the ionization process is neither strictly intensity dependent nor strictly energy-fluence dependent. The solid line, results from averaging $aI(x,t_{\text{cr}})$ over the interaction length for $I_{\text{peak}}=2.0\times10^{13}$ W/cm^2 and various pulse lengths, is energy-fluence dependent only and is asymptotically a limiting case to the semiempirical curve in the region of short-pulse duration. This is because under the influence of laser pulses of duration comparable with the time between electron-atom collisions, the electron drift velocity is strictly linearly proportional to the laser field. Our maximum ionization rate at t_{cr} (closed circles) corresponding to the current experimental conditions is 4.3×10^{13}/s.

In Fig. 7 we display in greater detail snapshots of electron density at times t_{cr} (solid curve) and $t_{\text{cr}}+0.5$ ps (dashed curve) in the bulk region ($x>0.1$ μm). The surface overdense layer region (not shown in the figure), not treated by the model after it is formed, is thought to be of order 0.1 μm, which is many optical skin depths. At t_{cr} the thickness of the bulk plasma region ($\geq10^{18}$ cm^{-3}) at the surface is $=\Delta t v_g=28$ μm. The shoulders in the density curves correspond to the moving ionization front whose time-dependent slope is sensitive to the pulse rise time near the critical threshold. Also shown are curves

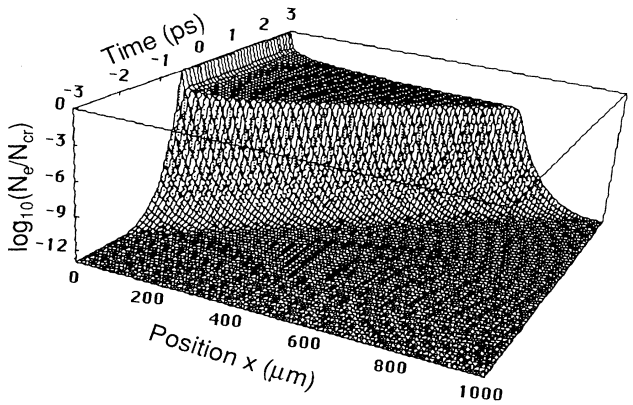

FIG. 5. Evolution of electron density behind the transparent target surface. Negative (positive) time is when the leading (trailing) edge of the pump pulse arrives at the surface ($x=0$). Zero time corresponds to the peak of the pulse at the surface.

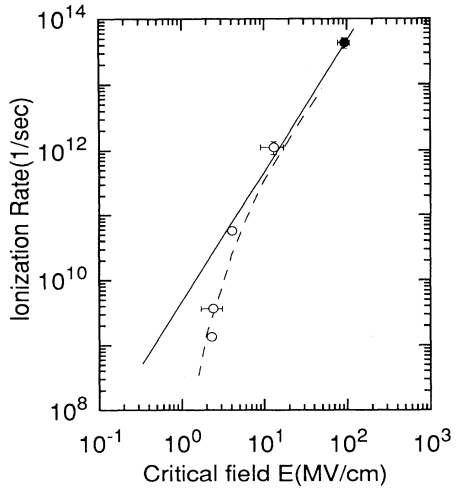

FIG. 6. Ionization rates as a function of critical or breakdown threshold field. Experimental points (open circles) and semiempirical calculation (dashed curve) are taken from Bloembergen [24] for comparison with the spatially averaged rates (solid line) given by Eq. (2). The solid circle corresponds to calculation based on the current experimental conditions. (See Bloembergen [24] for a more detailed discussion of the semiempirical curve.)

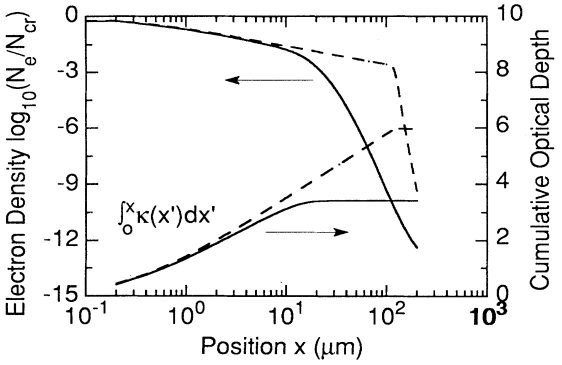

FIG. 7. Shown in greater detail, electron density profiles and cumulative optical depths as functions of position at times t_{cr} (solid curves) and at $t_{cr}+0.5$ ps (dashed curves).

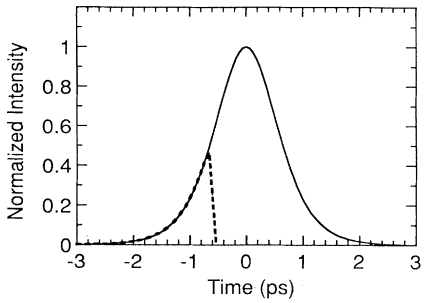

FIG. 8. Profile of the input pump pulse at the surface (solid curve) taken as sech^2 with 1.2-ps FWHM, and profile of the transmitted pulse at the rear surface (dashed curve) resulting in shorter FWHM and lower peak intensity. Note the zero point in transmitted pump profile occurs about 0.05 ps prior to the critical time $t_{cr}=-0.46$ ps.

for the cumulative optical depth [defined as $\int^x \kappa(x')dx'$], describing the spatial distribution of the bulk absorption.

The profile of the calculated transmitted pulse (dashed curve) exiting at the rear surface plotted in Fig. 8 is compared to that of the input pulse (solid curve) at the front surface, showing clearly the timing of maximum absorption of the transmitted pump energy. Note the zero-intensity point in the transmitted pump pulse occurs about 0.05 ps prior to t_{cr}. The sudden decrease in the transmitted pump pulse profile due to the rapid buildup of plasma density has been observed previously and used to determine breakdown threshold electric fields with pulses of many ps [24,25]. At t_{cr} decoupling of the transmitted and reflected pump pulses should be completed by the surface overdense plasma, and subsequently, the pump reflection should be increased strongly, which forms the basis of the plasma mirror effects [31]. We note that for Au-coated targets the intensity for critical plasma formation ($I_{cr}\approx 4\times 10^{11}$ W/cm^2) occurs about 1 ps earlier and at an intensity about 30 times lower than that in uncoated targets. Hence, bulk absorption at this level, as is shown in Fig. 8, is indeed negligible.

We now model the probe-pulse absorption. Absorption of the probe light is by e-atom inverse bremsstrahlung and obeys Beer's law. Considering a δ-like slice of the probe pulse entering the interaction region and reaching the front surface at time t prior to the critical time, $t<t_{cr}$, the probe time-dependent transmission and reflection are given by

$$T(t)=T_g \exp\left[-\int_0^{L_i}\kappa(x,t-n_0x/c)dx\right],$$
$$R(t)=R_g \exp\left[-\int_0^{L_i}\kappa(x,t-n_0x/c)dx - \int_0^{L_i}\kappa(x,t+n_0x/c)dx\right], \quad (3)$$

where T_g and R_g are the transmissivity and reflectivity of the cold glass target, and $L_i=100$ μm is the interaction length. The second exponential term in R accounts for additional absorption by the reflected probe pulse during its return journey.

For time $t\geq t_{cr}$ transmission of the probe is stopped, and probe reflection is modified by the formation of the surface plasma layer:

$$T\approx 0,$$
$$R(t)=R_s \exp\left[-\int_0^{L_i}\kappa(x,t-n_0x/c)dx - \int_0^{L_i}\kappa(x,t+n_0x/c)dx\right], \quad (4)$$

where R_s is the reflectivity of the surface overdense plasma layer. Previous experimental measurements of reflectivity with sub-ps pulses have shown that surface reflectivity range from 35% to 85% is possible [1,32]. Our estimates from Fresnel calculations of the surface reflectivity give a value of $\approx 40\%$ for R_s, which will be treated as a constant in a time scale of few ps, as was seen with Au-coated targets in Fig. 4. The above expressions are for instantaneous values, which are then convolved over the finite duration of the probe pulse.

To obtain least-square best fits to the data for uncoated targets, shown as solid curves in Fig. 3, we have used a pulse length of 1.2-ps FWHM, 0.2 ps longer than the recorded autocorrelation shown in Fig. 1. The most probable justification for this discrepancy is ascribed to variations in the pump-pulse intensity across the focal diameter, which translates into a range of critical times across the diameter of the plasma (see the Appendix). This spatial dependence of intensity was not accounted for by the model. The competition between the bulk plasma and the surface plasma is characterized by a relation between values of b and R_s that produce best fits to the experimental data. In Fig. 9 calculated values of b are plotted as a function of R_s (open-square curve) which give us estimates for the lower and upper limits of the cross section b for photon absorption. We note that values of b range within a factor of 3 for a reasonable

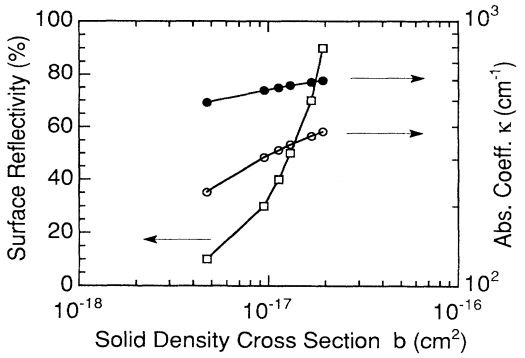

FIG. 9. Correlated values of surface overdense plasma reflectivity and solid density cross section (square-circle curve) that give best fits to the experimental reflectivity and transmissivity data. Also plotted are the corresponding absorption coefficient at t_{cr} (open-circle curve) and at $t \geq t_{cr}+0.5$ ps (close-circle curve).

range in R_s (10–70%). The average value of b of $\approx 1.0\times10^{-17}$ cm^2 is about five times lower than that predicted by Browne's formula, where it was derived for plasma formation in gas [19]. We attribute this reduction to the band structure and quantum transport effects in SiO_2 solid [33]. Also, the absorption coefficients of the bulk plasma, averaged over the interaction length, are plotted on the right scale against the values of b at time t_{cr} (open-circle curve) and at time $t \geq t_{cr}+L_i n_0/c = t_{cr}+0.5$ ps, the time when the density plateau begins to extend beyond the interaction region (closed-circle).

Another demonstration of the absorptive effect of the bulk underdense plasma on the measured reflection and transmission of the probe light can be shown by repeating the calculations without a bulk plasma. As one would expect from this calculation, there is no time lag between the transients of the reflectivity and transmissivity, and, more importantly, there is a reflectivity enhancement rather than a decrease as was observed. Thus, had the bulk plasma not been produced in uncoated targets, we would have seen a large reflection enhancement, as was shown with Au-coated targets in Fig. 4.

V. CONCLUSION

We have reported time-resolved measurements of the reflectivity and transmissivity of plasmas produced by intense ps-laser-pulse irradiation of initially transparent targets. The results demonstrate that before the peak of the pulse, there is a large underdense plasma formed in the bulk glass region which gives rise to absorption of the probe light. At subsequent times there is also an overdense plasma layer formed at the surface which prevents further transmission of the laser light and thus any subsequent increase in the plasma density and temperature in the bulk region. The data show competition of two opposing mechanisms: one is reflection by the surface overdense plasma, the other is absorption by the bulk underdense plasma. Experimental results for targets overcoated with a gold thin film showed that the bulk plasma can be eliminated as predicted. Moreover, related to the unsolved issues of previous works on laser-induced breakdown of optical materials [34], our experimental findings of the underdense plasma imbedded in the solid may very well be the direct evidence for avalanche buildup of charge in the bulk region. Time-resolved studies of the surface plasma and the bulk plasma provide dynamical pictures for different processes that lead to surface and bulk damages that have been seen in wide variety of optical materials [26,34].

We also have presented a model for plasma evolution in transparent materials with laser pulses of arbitrary shape. The model omits several physical processes, as were justified by their characteristic times that are irrelevant to the time scale of the experiment. These omissions are necessary to render simplicity and analyticity of the model, and at the same time, to retain the physical features similar to some previous models and preserve the characteristics of the well-known avalanche model. Moreover, unlike others, our model supplementally and self-consistently describes the characteristics of the high-intensity laser-pulse propagation in the target medium as it is absorbed by e-atom inverse bremsstrahlung, and it determines the growth rate, size, and absorptivity of the bulk plasma produced by the laser pulse. Also, it estimates the maximum amount of laser energy that can be transmitted through a transparent medium (see the Appendix), which is critical in studies of optical breakdown and the technology of high-power propagation in optical materials. The simplicity of the model allows one to perform rapid simulations on personal computers, and opens up ways for both time-resolved and integrated predictions of plasma dynamics in transparent solid materials. In particular, the model is useful for predicting the formation of relativistic underdense ionization fronts, which are of current interest for frequency upshifting [35,36].

Calculations of the reflected pump energy and pulse profile can also be obtained by energy conservation, but they will be somewhat overestimated, since the model does not include absorption of the pump energy by the overdense plasma layer at the front surface and its subsequent expansion into vacuum. These calculations, nevertheless, prove the possibilities for further investigation of time-resolved breakdown or plasma formation in transparent materials. All of these calculated parameters for the pump pulse, except t_{cr}, can be directly obtained from experiments. Information about the critical time, however, can be determined from comparison of the transmitted and reflected pulse profile with the incident pump; for example, by high-order autocorrelators. Concerning plasma mirror effects, the above calculations show that recording of the energy and profile of the transmitted pump pulse rather than the reflected pump pulse is more meaningful in that they are devoid of complications due to the effects of hydrodynamic expansion at the front surface. Furthermore, since most of the laser absorption is predicted to occur 0.14 ps prior to the critical time, the transmitted pump profile should allow us to determine the critical time and intensity threshold with an accuracy better than half of the laser pulse FWHM.

ACKNOWLEDGMENTS

We gratefully acknowledge A. Hazi and R. Bauer for their strong support of the project and M. Campbell for providing us laser time and some experimental apparatus. One of us (B.-T. Vu) thanks B. Chang for useful discussion of the model. We also wish to thank I. Thomas for the antireflection coatings and E. Pierce for the gold coatings. This work was performed under the auspices of the U.S. Department of Energy by Lawrence Livermore National Laboratory under Contract No. W-7405-ENG-48.

APPENDIX: CHARACTERISTICS OF PUMP LASER PULSES

By time integrating Eqs. (1) and (2) and employing the relations $I(\pm\infty)=0$ we obtain the time-integrated solution for the transmitted pump fluence:

$$\varepsilon(x)=-\frac{1}{a}\ln\left[\exp\left[-b\int_0^x N_{e0}(x')dx'\right]\times[\exp(-a\varepsilon_{cr})-1]+1\right], \quad \text{(A1)}$$

where $\varepsilon(x)=\int_{-\infty}^{+\infty} I(x,t')dt'$ is the transmitted energy fluence and $\varepsilon_{cr}=\int_{-\infty}^{t_{cr}} I(0,t')dt$ is the input fluence up to t_{cr} at the surface.

The critical time as the function of the peak intensity of the input pump pulse is plotted in Fig. 10. This curve is analytically obtained by setting the solution (2′) at the target surface, $N_e(0,t_{cr})=N_{cr}$. As expected, when the peak intensity is lowered, formation of the overdense plasma layer takes place progressively later along the pulse profile. This dependence is, though pulse-shape dependent, similar to the result from the avalanche model, where the breakdown intensity threshold is proportional to reciprocal of the laser pulselength [24,25]. At peak intensities $\leq 6\times10^{12}$ W/cm^2, critical plasma is formed during the trailing edge of the pulse and a small fluctuation in the intensity will result in a large change in the critical time, leading to large fluctuations in probe data. At higher intensities, by contrast, critical time occurs during the leading edge and a small peak intensity fluctuation leads to only a small change in the critical time, as is the case seen in Figs. 3 and 4. Figure 10 also shows calculated and measured transmitted pump energies as functions of incident peak intensity. The measured values each are averaged from 100 laser shots. The calculated values have been averaged over a factor of 4 in intensity to simulate transverse variations in the pump intensity. As is expected, when the peak intensity is low, most of the energy during the pulse is transmitted and little is reflected, and conversely when the peak intensity is high enough, the overdense plasma layer occurs early during the leading edge, allowing little light to pass.

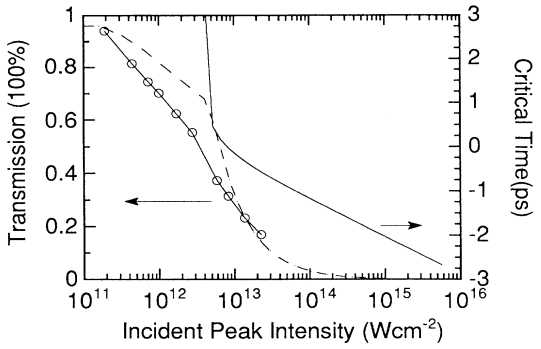

FIG. 10. Calculated critical time t_{cr} (solid curve), transmissivity T (dashed curve), and experimentally measured transmissivity (open-circle curve) of the pump pulse as functions of input peak intensity. Negative (positive) time corresponds to leading (trailing) edge of the pulse. Zero time is when the peak arrives at the surface.

[1] M. M. Murnane, H. C. Kapteyn, M. D. Rosen, and R. W. Falcone, Science **25**, 531 (1991).

[2] R. W. Falcone and M. M. Murnane, in *Short Wavelength Coherent Radiation: Generation and Applications,* edited by A. T. Attwood and J. Bokor (AIP, Monterey, CA, 1986), p. 81.

[3] M. D. Rosen, in *Femtosecond to Nanosecond High Intensity Lasers and Applications,* edited by E. M. Campbell (SPIE, Bellingham, 1990), p. 160.

[4] D. G. Stearns, O. L. Landen, E. M. Campbell, and J. H. Scofield, Phys. Rev. A **37**, 1684 (1988).

[5] A. Zigler *et al.*, Opt. Lett. **16**, 1261 (1991).

[6] O. L. Landen, D. G. Stearns, and E. M. Campbell, Phys. Rev. Lett. **63**, 1475 (1989).

[7] R. Fedosejevs, R. Ottomann, R. Sigel, S. Szatmari, and F. P. Schafer, Phys. Rev. Lett. **64**, 1250 (1990).

[8] A. Caruso and R. Gratton, Plasma Phys. **11**, 839 (1969).

[9] D. H. Reitze, H. Ahn, and M. C. Downer, Phys. Rev. B **45**, 2677 (1992).

[10] W. L. Kruer, *The Physics of Laser Plasma Interaction* (Addison-Wesley, Redwood City, CA, 1988).

[11] R. M. More, Lawrence Livermore National Laboratory, Report No. UCRL-84991 Parts I & II, 1981.

[12] N. G. Basov *et al.*, *Heating and Compression of Thermonuclear Targets by Laser Beam* (Consultants Bureau, New York, 1986).

[13] M. D. Perry, O. L. Landen, J. Weston, and R. Ettlebrick, Opt. Lett. **14**, 42 (1989).

[14] O. L. Landen and A. Szoke, Opt. Lett. **16**, 590 (1991).

[15] Curtin Matheson Scientific Inc. Glass type: Erie 2957. Glass chemical compositions: 72.6% SiO_2, 14.3% NaO, 6.3% CaO, 4.1% MgO, 1.12% Al_2O_3, 1.16% KO, 0.3% SO_3, 0.03% Fe_2O_3, 0.05% TiO_2. Refractive indexes: n(480 nm)=1.5213, n(546 nm)=1.5170, n(644 nm)=1.5120.

[16] R. R. Alfano, P. L. Baldeck, F. Raccah, and P. P. Ho,

Appl. Opt. **26**, 3491 (1987).
[17] P. L. Baldeck, R. R. Alfano, and G. P. Agrawal, Appl. Phys. Lett. **52**, 1939 (1988).
[18] B.-T. V. Vu, A. Szoke, and O. L. Landen, Opt. Lett. (to be published).
[19] P. F. Browne, Proc. Phys. Soc. **86**, 1323 (1965).
[20] Y. B. Zeldovich and Y. P. Raizer, *Physics of Shock Waves & High Temperature Hydrodynamic Phenomena* (Academic, New York, 1966).
[21] M. M. Murnane, H. C. Kapteyn, and R. C. Falcone, Phys. Rev. Lett. **62**, 155 (1989).
[22] J. M. Dawson, Phys. Fluids **7**, 981 (1964).
[23] D. M. Fradin, E. Yablonovitch, and M. Bass, Appl. Opt. **12**, 700 (1973).
[24] N. Bloembergen, IEEE J. Quantum Electron. **QE-10**, 375 (1974).
[25] E. Yablonovitch and N. Bloembergen, Phys. Rev. Lett. **29**, 907 (1972).
[26] Y. R. Shen, *The Principals of Nonlinear Optics* (Wiley, New York, 1984).
[27] R. J. Harrach, Lawrence Livermore National Laboratory, Report No. UCRL-52389, 1977.
[28] M. Newstein and N. Solimene, IEEE J. Quantum Electron. **QE-17**, 2085 (1981).
[29] L. M. Frantz and J. S. Nodvik, J. Appl. Phys. **34**, 2346 (1963).
[30] S. C. Jones, A. H. Fischetti, P. Braunlich, and P. Kelly, Phys. Rev. B **37**, 755 (1988).
[31] H. C. Kapteyn, M. M. Murnane, A. Szoke, and R. W. Falcone, in *Ultrafast Phenomena VII,* edited by C. B. Harris, E. P. Ippen, and G. A. Mourou (Springer-Verlag, Berlin, 1990), p. 122.
[32] H. M. Milchberg, R. R. Freeman, S. C. Davey, and R. M. More, Phys. Rev. Lett. **61**, 2364 (1988).
[33] M. V. Fischetti, D. J. DiMaria, S. D. Brorson, T. N. Theis, and J. R. Kirtley, Phys. Rev. B **31**, 8124 (1985).
[34] W. Lee Smith, Opt. Eng. **17**, 489 (1978).
[35] H. C. Kapteyn and M. M. Murnane, J. Opt. Soc. Am. B **8**, 1657 (1991).
[36] W. B. Mori, Phys. Rev. A **44**, 5118 (1991).